Research Article

Received: 23 November 2022 Revised: 10 February 2023 Accepted article published: 28 February 2023 Published online in Wiley Online Library:

(wileyonlinelibrary.com) DOI 10.1002/jctb.7357

Systematic screening of carbon-based anode materials for bioelectrochemical systems

Zainab Ul,[a] Pilar Sánchez-Peña,[a] Mireia Baeza,[b] Mira Sulonen,[a] David Gabriel,[a] Juan Antonio Baeza[a*] and Albert Guisasola[a]

Abstract

BACKGROUND: The anode material of bioelectrochemical systems (BES) is crucial because its characteristics directly affect electron transfer from the bacteria to the anode. To assess its usefulness, each material must undergo evaluation under relevant operating conditions, as well as a complete electrochemical characterization.

RESULTS: Five carbonaceous materials – carbon brush (CB), carbon granules (CG), thicker carbon felt (CF1), high-conductivity carbon felt (CF2), and high-active-area carbon felt (CF3) – anodes were tested in this work. The current generation with each anode material was studied, operating as a microbial fuel cell (MFC) and microbial electrolysis cell (MEC). Two MFC inoculation strategies were tested: (i) fixed 10 Ω external resistance (ER) and (ii) poised anode potential (PA) of 200 mV *versus* Ag/AgCl. Once reproducible cycles were obtained in MFC operation, CB yielded the highest maximum current density, amounting to 15.9 A m^{-2}. A slightly reduced start-up time was observed for each anode with PA than ER. When the anodes were transferred to MEC operation, the maximum hydrogen production rate of 1.04 m^3 H_2 m^{-3} d^{-1} was obtained for CB.

CONCLUSION: This study helps in selecting anode material for BES, allowing a shortening of the start-up time and improving its performance using different inoculation strategies and anode materials. Among all the anode materials employed in this study, CB and CF3 electrodes presented the best overall performance.

Supporting information may be found in the online version of this article.

Keywords: carbon-based anode materials; microbial fuel cell (MFC); poised anode potential; microbial electrolysis cell (MEC); start-up time

INTRODUCTION

Among emerging energy and resource recovery concepts, microbial fuel cells (MFCs) have received significant attention. They are extensively studied, driven by the promise of renewable energy generation while treating wastewater simultaneously.[1] Considerable studies have been conducted concerning the improvements in reactor designs,[1,2] electrode materials,[3-5] enrichment of anode-respiring bacteria (ARB),[6] and optimization of process limits.[7] Even though impressive progress has been achieved, MFC still faces many challenges in its implementation in a commercial market.

Microorganisms can transform biochemical energy into adenosine triphosphate by a series of reactions in which electrons are eventually transferred to a terminal electron acceptor.[8] In the respiration performed by ARB, the electron acceptor is a solid anode. In MFCs, ARBs grow on the anode and oxidize organic matter anaerobically to produce carbon dioxide and release protons into the solution and electrons to the circuit. The electrons then travel through a wire to a cathode, reducing oxygen to water and generating electrical power.[9] The transfer of electrons from the microbe to the anode is critical in the whole system.[10-12] Soluble mediators, redox-active proteins or nanowires facilitate this extracellular electron transfer process (EET).[13] Nevertheless, the physical and chemical properties of the anode materials can also substantially influence the EET and, therefore, have a crucial impact on MFC overall performance.[14,15]

Anode material properties such as composition, morphology, and surface characteristics directly affect microbial adhesion, electron transfer, and substrate oxidation.[12] Consequently, the material should meet several criteria for suitability as an anode, such as high electrical conductivity, enhanced biocompatibility, high chemical and physical stability, reasonable cost, and availability.[16]

* *Correspondence to: JA Baeza, GENOCOV, Departament d'Enginyeria Química, Biològica i Ambiental, Escola d'Enginyeria, Universitat Autònoma de Barcelona, 08193 Bellaterra (Cerdanyola del Vallès), Barcelona, Spain. E-mail: juanantonio.baeza@uab.cat*

a *GENOCOV, Departament d'Enginyeria Química, Biològica i Ambiental, Escola d'Enginyeria, Universitat Autònoma de Barcelona, Barcelona, Spain*

b *GENOCOV, Departament de Química, Facultat de Ciències, Universitat Autònoma de Barcelona, Barcelona, Spain*

In general, three types of anode materials have been employed in MFCs: carbon, metal, and composite materials. So far, only carbon-based materials have been reported to have all or most desired characteristics and are, therefore, the most commonly used anodes.[6,17,18] Carbon-based electrodes have high chemical stability, low cost, good microbial adhesion, high porosity, and specific surface area, but lower electrical conductivity. Typical carbonaceous anodes are carbon felts (CF), carbon brushes (CB) and carbon granules (CG). CF and CB are extensively available, easy to operate, and can be supplied at a reasonable cost. CG benefit from filling a large anodic volume with good compactness, but CG must be packed tightly to ensure good current flow through all the granules and the current collector and to prevent short circuits to the cathode.

The anode potential also plays an essential role in BES since it regulates both electrical energy output and the theoretical energy gain for microorganisms, closely related to their growth rate and electron affinity.[15,19-21] Electrons are transferred from ARB to the anode because of the potential difference between the final electron carrier and the anode.[22] This potential difference influences the EET rate, given that electrons will be driven from a high to a low energy status.[23] Hence, the higher the anode potential, the more energy per electron transferred is available for cell growth and maintenance. From a thermodynamic perspective, the energy gain for the microorganisms can be calculated using Eqn (1):

$$\Delta G^{o\prime} = -nF\left(E_{\text{anode}} - E^{o\prime}_{\text{substrate}}\right) \quad (1)$$

where $\Delta G^{o\prime}$ (J mol^{-1}) denotes the Gibbs free energy under standard biological conditions (pH 7 and 25 °C), n is the number of electrons conveyed, F is the Faraday constant (96 485 C mol^{-1} e^{-1}), E_{anode} is the anode potential (V) and $E^{o\prime}_{\text{substrate}}$ represents the standard biological potential of the substrate (V).[24]

ARB will use this additional energy with more positive anode potentials, provided the cell can capture this energy by pumping extra protons outside the inner cell membrane.[25] Hence, the microorganisms must process metabolic pathways to use this additional free energy given by the anode. In these circumstances, anode potential should be positively associated with the current generation and increased biomass yields, depending on the microorganism's metabolic efficiency under these conditions.[13]

Several research groups have previously reported improved acclimation of exoelectrogenic biofilms in bioelectrochemical systems (BES) under poised anode (PA) potential, resulting in better performance and faster start-up time. Wang *et al.*[26] obtained reduced start-up time and higher current output by applying a positive anodic potential of 200 mV *versus* Ag/AgCl than the control MFC operated under 1000 Ω due to the increased driving force of substrate oxidation. The study reported by Wei *et al.*[21] showed that a considerable gain in biomass and power density was obtained when anode potential increased from −160 to 0 mV *versus* standard hydrogen electrode (SHE). However, no improvement in biomass and power output was observed when the anode potential further increased to 400 mV *versus* SHE.[21] More recently, Zhu *et al.*[27] observed that acclimating the biofilm with positive potentials may cause the decay of the power overshoot phenomenon, leading to improved power performance.[27] However, studies on the optimal value and effect of PA on BES performance have been inconclusive.

Therefore, considering these research trends, our objective was to identify carbon-based anode materials that yield high performance. It is challenging to compare anode material from the literature since the studies differ in operating conditions, measurement techniques, inoculation strategies, and cell design. Hence, experiments were carried out to determine the effect of different anode materials on BES performance. Concomitantly, two different start-up strategies of PA of +200 mV *versus* Ag/AgCl and 10 Ω external resistance (ER) to close the circuit were also

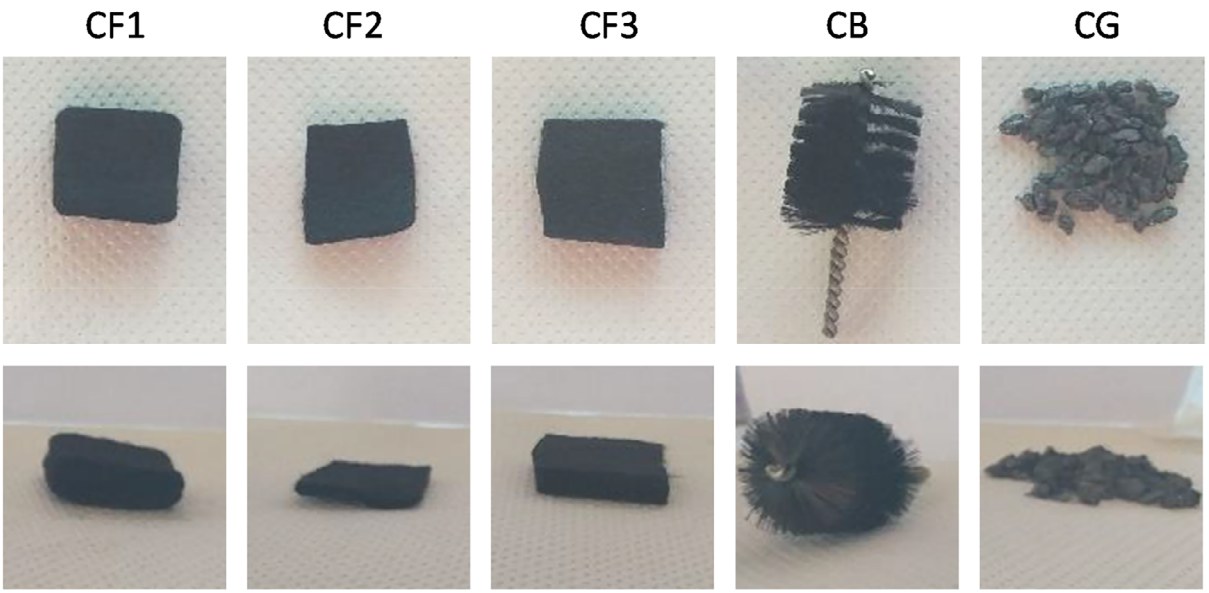

Figure 1. Carbon-based anode materials employed in this study: thicker carbon felt, CF1 (2 cm × 2 cm); high-conductivity carbon felt, CF2 (2 cm × 2 cm); high-active-area carbon felt, CF3 (2 cm × 2 cm); carbon brush, CB (2.5 cm length; 2 cm diameter); and carbon granules, CG (filled in cylindrically shaped body, 2.4 cm length; 1.5 cm diameter).

Journal of Chemical Technology and Biotechnology published by John Wiley & Sons Ltd on behalf of Society of Chemical Industry (SCI).

investigated. Different losses were characterized by polarization curves and electrochemical impedance spectroscopy (EIS) analysis. Cyclic voltammetry (CV) was also performed to evaluate the impact of varying anode materials on the electrode's electrochemical properties. This study investigates avenues for improving the anodic performance, emphasizing anode material and inoculation strategies.

EXPERIMENTAL

Cell description and medium composition

Single-chamber MFCs (28 mL) were assembled using cube-shaped methacrylate bodies (4.4 cm length × 5 cm width × 5 cm height), with two lateral methacrylate endplates through O-rings and gaskets to prevent liquid leakages. In MFCs, one of the endplates was perforated to allow oxygen transfer to the air cathode. In the MEC design, both ends were closed, thus enhancing anaerobic conditions. Hydrogen gas was sampled and collected via gas bags at the top of the MEC reactors.[28]

Five different carbon-based materials were tested (Fig. 1). Three different types of carbon felt (2 cm × 2 cm, 4 cm^2 of projected surface area) were used: CF1, CF2 and CF3, with a thickness of 6.1 mm, 2.4 mm and 3.9 mm, respectively. CF1 and CF2 anode materials were donated by Leitat Technological Center (Spain). The CF3 electrode was given by the National Hydrogen and Fuel-cell Technology Testing Center (Spain). The CB was made of graphite fibre, 20 mm diameter × 25 mm length; 0.18 m^2 fibres of 7.2 μm diameter (PANEX 33 160 K, ZOLTEK Corporation, Bridgeton, MO, USA) were wound into a titanium wire of 2 mm diameter. Before use, the brush was heat-treated in a furnace at 450 °C for about 30 min to increase the active area due to microfracture generation and thus enhance biomass adhesion. For CG, a cylindrically shaped body for the anode chamber was designed (24 mm in length and 15 mm in diameter) and printed with a 3D printer (BCN3D Sigma D25), in which approximately 3 g granules were filled. The filament used was a 2.85 mm thick dark-blue polylactic filament. The extrusion temperature was 210 °C, with a printing speed of 50 mm s^{-1} and a retraction speed of 35 mm s^{-1}. Carbon felt and CG electrodes were used as received, without further special treatment. Titanium wire was used as current collector for all electrodes. The projected surface area for each anode material is presented in Table 1.

Carbon cloth (7 cm^2) used as a cathode was painted, using a spray technique, with a powder containing 90% carbon and 10% platinum until a coating of 0.5 mg Pt cm^{-2} (Electrochem Inc., Woburn, MA, USA) was obtained on the inner side. The procedure of Middaugh *et al.* was followed to prepare the cathode.[29] The PTFE (polytetrafluoroethylene) diffusion layer applied on the outer side of the cathode allowed air diffusion into the MFC.[30]

The MFCs were inoculated with 14 mL of broth from an MFC with ARB-enriched biomass, 14 mL fresh mineral medium and acetate at a final concentration of approximately 1.5 g L^{-1}. The mineral medium stock solution (pH 7) contained (per litre): 12.04 g Na_2HPO_4, 2.06 g KH_2PO_4, 0.2 g NH_4Cl, 4.0 mg $FeCl_2$, 6.0 mg Na_2S and 5 mL of a nutrient solution containing (g L^{-1}): 1 EDTA, 0.164 $CoCl_2.6H_2O$, 0.228 $CaCl_2.2H_2O$, 0.02 H_3BO_3, 0.04 $Na_2MoO_4.2H_2O$, 0.002 Na_2SeO_3, 0.02 $Na_2WO_4.2H_2O$, 0.04 $NiCl_2.6H_2O$, 2.32 $MgCl_2$, 1.18 $MnCl_2.4H_2O$, 0.1 $ZnCl_2$, 0.02 $CuSO_4.5H_2O$ and 0.02 $AlK(SO_4)_2$.

Start-up strategies

Ten reactors in total were operated in batch mode to evaluate both strategies. In the first one, five MFCs were employed to perform experiments using a 10 Ω ER and titanium wires to close the circuit (Fig. 2(A)). The voltage across the ER was monitored using a 16-bit data acquisition card (Advantech PCI-1716) connected to a computer with AddControl software developed by the authors with LabWindows/CVI 2020 for data acquisition.[31]

In the second strategy, the other five cells were operated with PA at +200 mV *versus* Ag/AgCl reference electrode (3 mol L^{-1} KCl RE-1B, +210 *vs.* SHE, BAS Inc., Tokyo, Japan) by connecting the potentiostat to the anode as working electrode and to the cathode as a counter electrode (Fig. 2(B)). The anode potential was fixed using a multichannel potentiostat (Whistonbrook Technologies, Luton, UK), and the resulting current was recorded every minute.

The cells were considered to operate after the current exceeded 0.5 mA for the first time. Once a stable current was obtained for carbon-based anodes working with ER, the anodes were transferred to hydrogen-producing MECs with an applied voltage of 1.2 V.

Analyses

Acetate concentration was measured at the beginning and end of each cycle with a gas chromatograph (model 7820-A, Agilent Technologies, Santa Clara, CA, USA) employing a DB-FFAB column (30 m length, 250 μm internal diameter and 0.25 μm film thickness) and a flame ionization detector. The sample preparation procedure consisted of pipetting 800 μL of filtered samples (0.22 μm syringe filter) in a glass vial with 200 μL preserving solution (used as an internal standard). The preserving solution was composed of 2 g $HgCl_2$, 2 g hexanoic acid and 33.7 g orthophosphoric acid in 1 L deionized water.

Hydrogen was quantified with gas chromatography using an HP-Molesieve column (30 m × 320 μm × 12 μm; length × internal diameter × film thickness) and a thermal conductivity detector. The run time was 6 min.

Table 1. Projected surface area for the five anode materials and parameters obtained/calculated from different electrochemical techniques

		CV		EIS		Polarization curve	
Anode material	Projected surface area (cm^2)	Redox peaks	Electroactive area (cm^2)	R_Ω (Ω)	R_{ct} (Ω)	R_{int} (Ω)	Maximum power (W)
CF1	4	(0.37 V; 0.08 V)	0.03	1.83	9.23	185	438
CF2	4	—	n.d.	4.13	5.07	237	442
CF3	4	(0.25 V; 0.18 V)	2.93	4.11	2.60	122	835
CB	5	(0.25 V; 0.20 V)	2.02	3.26	6.19	111	751
CG	3.6	(0.27 V; 0.19 V)	1.81	3.89	3.21	179	441

Abbreviations: CF1, thicker carbon felt; CF2, high-conductivity carbon felt; CF3, high-active-area carbon felt; CB, carbon brush; CG, carbon granules; CV, cyclic voltammetry; EIS, electrical impedance spectroscopy; R_Ω, ohmic resistance; R_{ct}, charge transfer resistance; R_{int}, internal resistance.

Journal of Chemical Technology and Biotechnology published by John Wiley & Sons Ltd on behalf of Society of Chemical Industry (SCI).

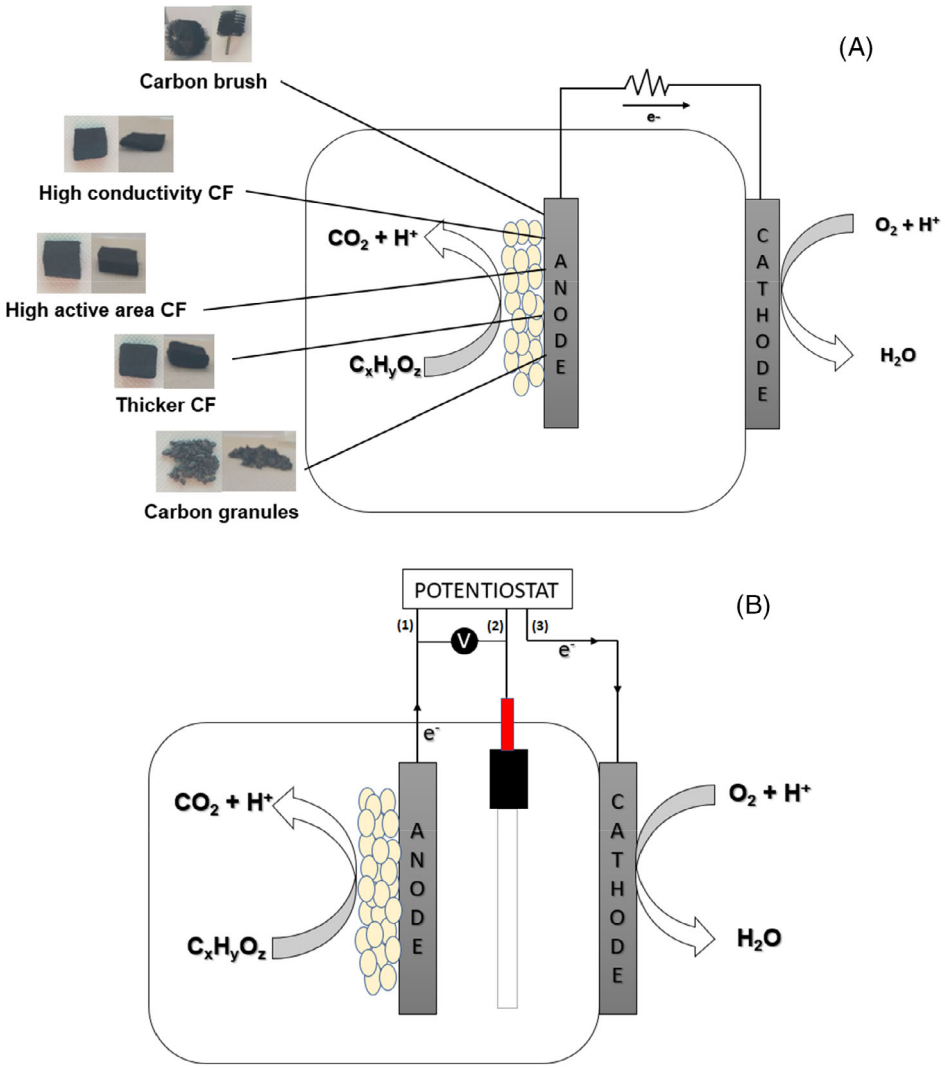

Figure 2. Schematic diagram of (A) microbial fuel cell employing an external resistance and (B) microbial fuel cell with poised anode potential of +200 mV: (1) working electrode; (2) reference electrode; and (3) counter electrode.

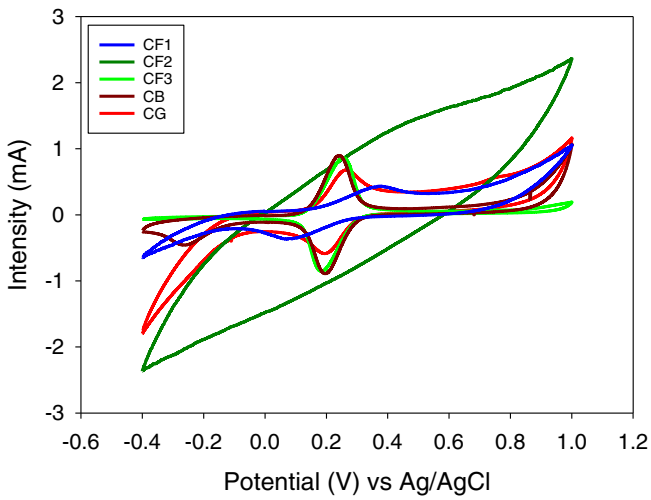

Figure 3. Cyclic voltammetry with different anode materials. Scan rate: 0.001 V s^{-1}; solution media contained 0.01 mol L^{-1} ferro/ferricyanide; the anode was the working electrode and the cathode was the counter electrode against Ag/AgCl, 3 mol L^{-1} KCl reference electrode. CF1, thicker carbon felt; CF2, high-conductivity carbon felt; CF3, high-active-area carbon felt; CB, carbon brush; CG, carbon granules.

Journal of Chemical Technology and Biotechnology published by John Wiley & Sons Ltd on behalf of Society of Chemical Industry (SCI).

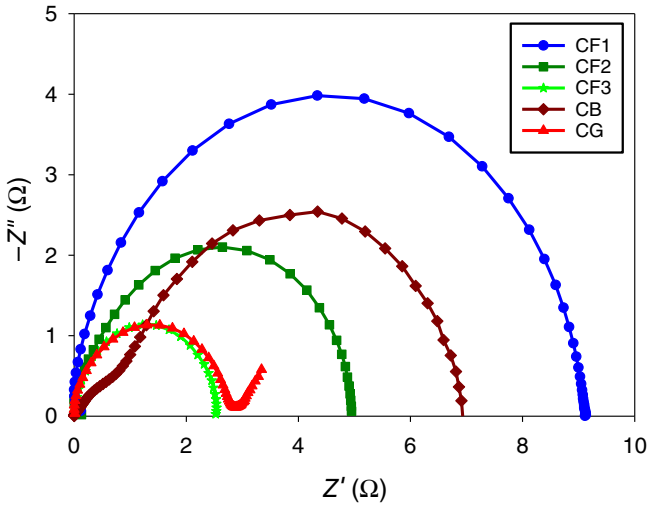

Figure 4. Nyquist plots obtained using electrochemical impedance spectroscopy with different anode materials. CF1, thicker carbon felt; CF2, high-conductivity carbon felt; CF3, high-active-area carbon felt; CB, carbon brush; CG, carbon granules.

Duplicate samples were collected for microbial community characterization from the surface of the carbon-based anode electrodes after PA operation for 50 days. DNA was extracted using a Soil DNA Isolation Plus Kit (Norgen Biotek, Thorold, ON, Canada) following the manufacturer's instructions. The quantity and integrity of the extracted DNA were checked with an ND-1000 Nanodrop spectrophotometer (Thermo Fisher Scientific, Waltham, MA, USA), and the samples were stored at −80 °C before amplicon sequencing. To profile the microbiome composition, the V4 region of the 16S rRNA genes was sequenced (using primers with 515F and 806R) on the Illumina MiSeq platform (2 × 300 bp paired-end) at RTL Genomics (Lubbock, TX, USA).

System performance indexes

The current density with respect to the anode was calculated based on the projected surface area and also on the electroactive area. The bioelectrochemical process efficiency was estimated in terms of coulombic efficiency (%), cathode hydrogen recovery (%), and volumetric hydrogen production rate per volume of cell (m^3 H_2 m^{-3} d^{-1}). Coulombic efficiency (Eqn 2) is the ratio between electron moles extracted as current intensity to the total electron moles made available from substrate oxidation.

$$CE = \frac{\int_{t_0}^{t_F} I\,dt}{\left(F\,b_s\,V_L\,\Delta C\,M_s^{-1}\right)} \times 100 \quad (2)$$

where t_0 and t_F (s) are the initial and final times of a batch experiment, I (A) is current, F (96 485 C mol^{-1} e^-) represents Faraday's constant, V_L (mL) is the volume of liquid in the reactor, M_s (g mol^{-1}) is the molecular weight of the substrate, b_s is the number of e^- transferred per mole of the substrate, and ΔC (g L^{-1}) is equal to the difference between initial and final substrate (in this work, acetate) concentration over a batch cycle.

MEC performance was also assessed by employing the cathodic gas recovery (r_{cat}), which compares the coulombs theoretically consumed to produce the measured hydrogen with the coulombs arriving at the cathode as current intensity (Eqn 3).

$$r_{cat} = \frac{V_{H_2}\,b_{H_2}\,F\,V_m^{-1}}{\int_{t_0}^{t_f} I\,dt} \times 100 \quad (3)$$

where V_{H2} (L) is the volume of produced hydrogen, b_{H2} (2 mol e^- mol^{-1} H_2) is the number of moles of e^- transferred per mole of hydrogen, and V_m (24.03 L mol^{-1}) is the molar gas volume at 20 °C.

Electrochemical techniques

Cyclic voltammetry

In three-electrode mode, CVs were conducted using a Multi Auto lab system (Ecochemie, Utrecht, Netherlands). A potential ramp over the range from −0.4 V to 1.2 V, at a scan rate of 0.001 V s^{-1}, was applied to the working electrode (abiotic anode) by gradually increasing the potential and then reversing the scan returns to the initial potential. All the electrochemical assays were performed in 0.01 mol L^{-1} ferro/ferricyanide solution by considering the anode as a working electrode and cathode as a counter electrode against Ag/AgCl, 3 mol L^{-1} KCl reference electrode. The electroactive area of the electrodes was calculated using the Randles–Sevick equation (Eqn 4).

$$i_p = 0.4463\left(\frac{n^3 \cdot F^3}{RT}\right)^{\frac{1}{2}} A\,C\,(D\,v)^{\frac{1}{2}} \quad (4)$$

where i_p is peak current (A), n is number of electrons transferred in a redox cycle, R is the universal gas constant (8.31 J K^{-1} mol^{-1}), T is temperature (K), A is the electrode active area (cm^2), C is the molar concentration of redox active species (mol cm^{-3}), D is the diffusion coefficient (cm^2 s^{-1}) and v is the scan rate (V s^{-1}).

Electrochemical impedance spectroscopy

EIS was measured by employing a multi-Autolab system (model PGSTAT204, Metrohm, Herisau, Switzerland) using a three-electrode configuration so that the abiotic anode was the working electrode and the cathode was the auxiliary one. An Ag/AgCl, 3 mol L^{-1} KCl electrode was used as a reference electrode. EIS measurements were recorded at the cell open-circuit voltage (OCV) frequency range from 100 kHz to 10 MHz. All the EIS curves

Journal of Chemical Technology and Biotechnology published by John Wiley & Sons Ltd on behalf of Society of Chemical Industry (SCI).

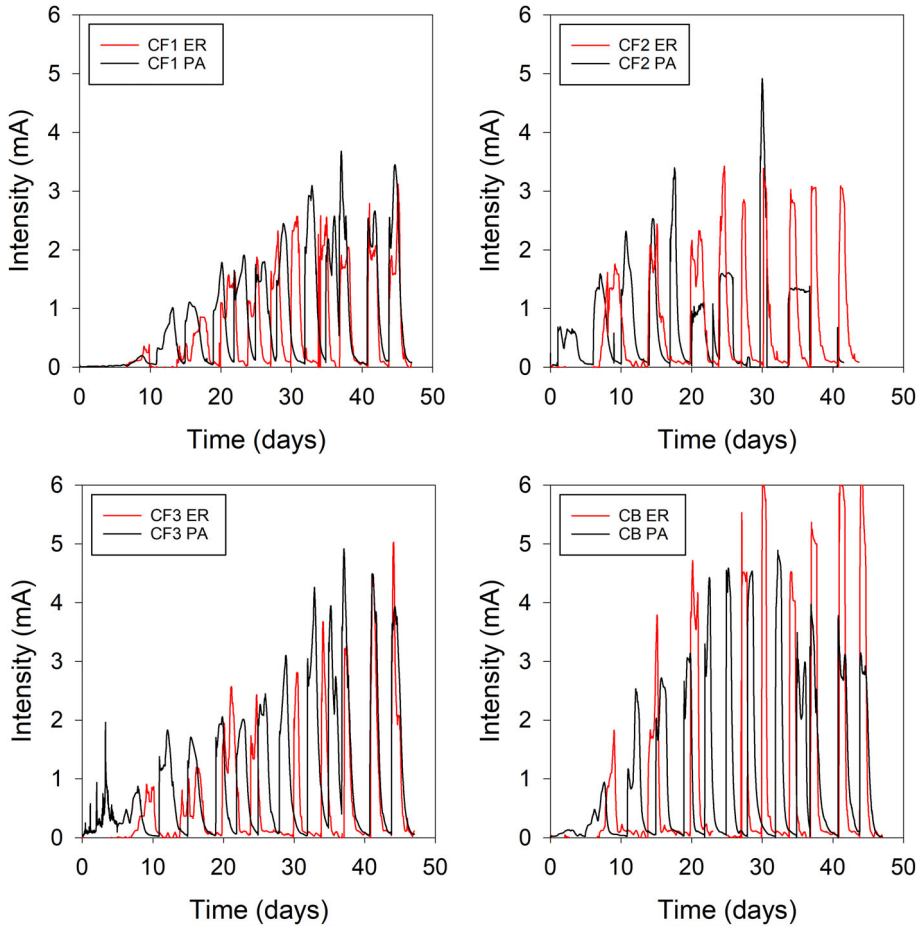

Figure 5. Current outputs during start-up of microbial fuel cells. CF1, thicker carbon felt; CF2, high-conductivity carbon felt; CF3, high-active-area carbon felt; CB, carbon brush; ER, external resistance; PA, poised anode potential.

Table 2. System performing indexes obtained from different inoculation strategies

	Start-up strategy	Maximum intensity (mA)	CE (%)	Days for current generation
CF1	ER	3.1	79	15
	PA	3.5	88	12
CF2	ER	3.4	83	7
	PA	4.8	72	2
CF3	ER	5.0	74	8
	PA	4.5	98	3
CB	ER	6.6	65	9
	PA	4.9	88	5

Abbreviations: CF1, thicker carbon felt; CF2, high-conductivity carbon felt; CF3, high-active-area carbon felt; CB, carbon brush; ER, external resistance; PA, fixed anode potential; CE, coulombic efficiency.

obtained were equivalent to the characteristic Nyquist plot and were adjusted to the Randles circuit. In the Nyquist plot, the high-frequency limit impedance is the ohmic resistance (R_Ω), whereas the semicircle's diameter represents the charge transfer resistance (R_{ct}).[1] The R_{ct} was estimated as the absolute value of the semicircle's intercept with the real axis at low frequencies minus the electrolyte resistance found in the intercept with the real axis at high frequencies. Therefore, the impedance at the low-frequency limit includes both resistances (R_Ω + Rct). For the EIS tests, the solution medium contained 0.1 mol L^{-1} KCl, 0.01 mol L^{-1} $K_4(Fe(CN)_6)$ and 0.01 mol L^{-1} $K_3(Fe(CN)_6)$.

Polarization curves

Polarization curves were obtained using a multi-resistance board and measuring the voltage. The set of 17 ER used was in the range 470 kΩ to 25 Ω. The medium was renewed before recording polarization curves to ensure enough substrate was available during the experiments. Once a steady-state current was obtained, the cells were left in open circuit for 30 min. After that, the voltage over each resistance was recorded employing a multimeter (every resistor was tested for 15 min). The current output was then calculated through Ohm's law and power by Eqn (5):

Journal of Chemical Technology and Biotechnology published by John Wiley & Sons Ltd on behalf of Society of Chemical Industry (SCI).

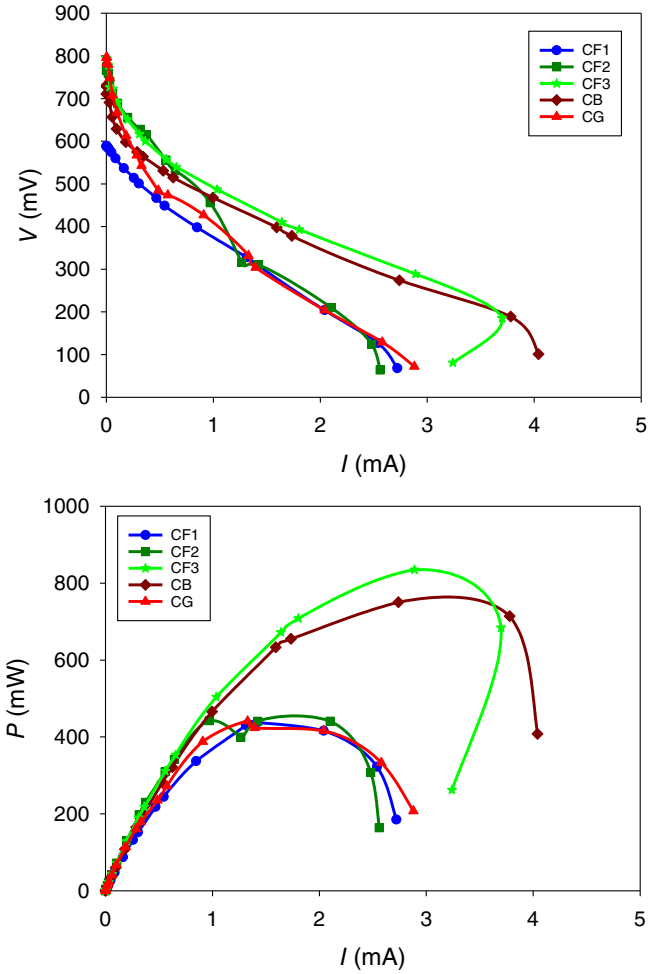

Figure 6. Polarization (A) and power curves (B) for different anode materials. CF1, thicker carbon felt; CF2, high-conductivity carbon felt; CF3, high-active-area carbon felt; CB, carbon brush; CG, carbon granules.

Table 3. System performing indexes for different anodes in MFC

	Maximum current (mA)	Maximum power (mW)	CE (%)	J_{EA} (A m^{-2})[a]	J_{PA} (A m^{-2})[b]
CF1	3.2	102	82	73.2	8.0
CF2	3.3	111	72	-	8.3
CF3	5.7	325	94	18.4	14.3
CB	7.0	480	85	35.7	15.9
CG	3.5	125	60	18.3	9.7
CF3 circularly stacked	7.2	518	79	-	16.4

Abbreviations: CF1, thicker carbon felt; CF2, high-conductivity carbon felt; CF3, high-active-area carbon felt; CB, carbon brush; CG, carbon granules; CE, coulombic efficiency.
[a] Current density normalized with respect to electroactive area.
[b] Current density normalized with respect to projected surface area.

$$P = V I \quad (5)$$

where P (W) is the power output.

Morphological characterization using SEM

The biofilm structure of each anode material inoculated with PA was visualized on an SEM instrument using a MerlinZeiss microscope operated at 5 kV and with an energy dispersive X-ray analysis system and (model JSM 6010, JOEL Ltd, Tokyo, Japan).

RESULTS AND DISCUSSION

The results of this study are organized as follows. The anode materials were evaluated under abiotic conditions with cyclic voltammetry (first subsection) and EIS (second subsection) to

Journal of Chemical Technology and Biotechnology published by John Wiley & Sons Ltd on behalf of Society of Chemical Industry (SCI).

Table 4. System performing indexes for different anodes in MEC

	Maximum intensity (mA)	Hydrogen production rate ($m^3\ m^{-3}\ d^{-1}$)	CE (%)	r_{cat} (%)
CF1	3.5	0.56	61	67
CF2	4.9	0.68	68	80
CF3	3.6	0.88	73	98
CB	7.5	1.04	85	90
CG	7.2	0.78	81	65
CF3 circularly stacked	7.3	0.92	78	99

Abbreviations: CF1, thicker carbon felt; CF2, high-conductivity carbon felt; CF3, high-active-area carbon felt; CB, carbon brush; CG, carbon granules; CE, coulombic efficiency; r_{cat}, cathodic gas recovery.

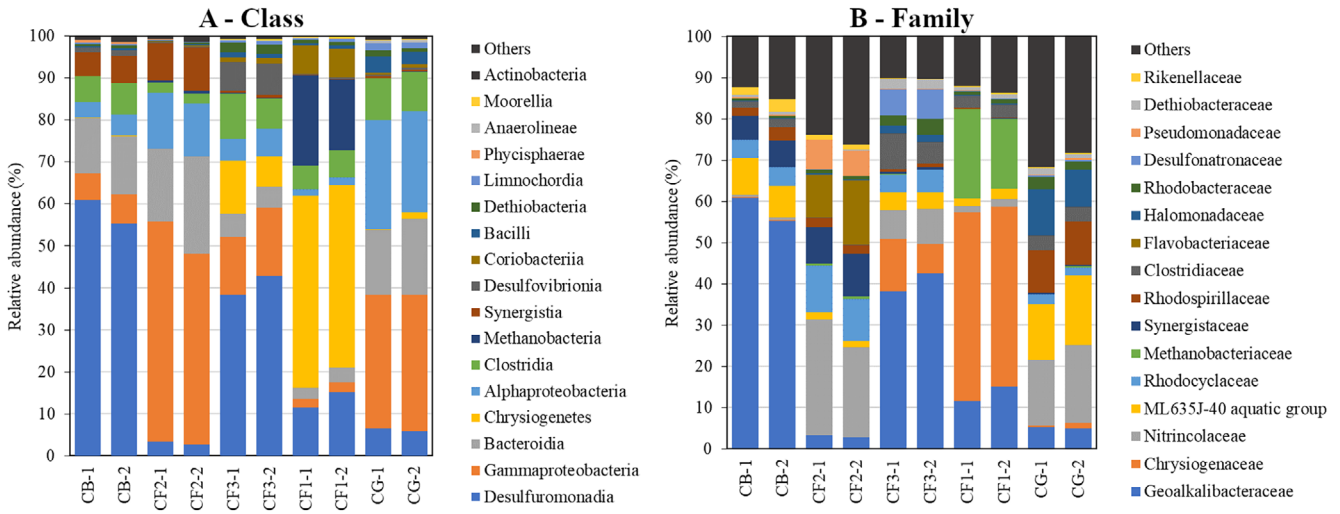

Figure 7. Microbial analysis for different carbon-based anodes.

understand their electrochemical behaviour before inoculation. The third subsection shows the performance of the MFCs obtained during the start-up period. The performance of the anode materials after the stable operation is analysed with polarization curves in the fourth subsection. The long-term MFC performance is shown in the fifth subsection and MEC Performance in the sixth subsection. Finally, the seventh subsection summarizes the microbial and the eighth subsection the SEM characterization of the anodes.

Cyclic voltammetry

The anode materials were evaluated by abiotic CV tests to identify the best one in terms of lowest overpotential and highest current generation. The results are presented in Fig. 3 as current and Supporting Information Fig. S1 as current density. Different characteristics of the anode material affected the positions and sizes of the redox peaks. The behaviour of CF2 was different from the others because no valuable overpotentials were detected for the CF2 electrode due to its capacitive behaviour. The CVs for CF3, CB and CG presented the fastest electron exchange rate at the electrode surface. These electrodes showed a single pair of well-developed reversible redox peaks, suggesting that a single-step electrochemical reaction occurred on the anode. Although CF1 presented a reversible behaviour, it was less than the other electrodes as the distance between anodic and cathodic peaks increased. Moreover, CF3, CB and CG peak-to-peak separation (Table 1) was much smaller than the other electrodes, revealing an electrochemical behaviour closer to reversibility and indicating rapid electron transfer kinetics. CB's pair of redox peaks were those with lower separation (0.25 V; 0.20 V). The overpotential of CB, CF3 and CG was much lower than the overpotential shown by the CF1 electrode. These results suggest that CB, CG and CF3 proved to be better since they required a lower voltage for high current generation.

The abiotic CVs were also useful to calculate the electroactive area (Table 1), showing the best results of 2.93 cm^2 for CF3, followed by CB (2.02 cm^2) and CG (1.81 cm^2). CF3 and CB also produced the highest maximum peak intensity of the carbonaceous materials employed in this study, which points to enhanced electrocatalytic anode activity, likely due to the increased electroactive surface.

Electrochemical impedance spectroscopy

The impedance spectra allow a broad overview of the different processes at the electrochemical interface of the anode, not at the complete electrochemical cell. In this method, the system is perturbed with an alternating current of small magnitude and the way the system behaves is studied at a steady state. It must be considered that the rest of the variables remain constant (auxiliary electrode (cathode), external resistance, resistance to the flow of electrons through the rest of the cell, etc.) so that, although these resistances are essential to define the interfacial

Journal of Chemical Technology and Biotechnology published by John Wiley & Sons Ltd on behalf of Society of Chemical Industry (SCI).

process on the surface of the anode, their contribution to the internal resistance of the cell is consistent.

In this study, all anode R_Ω were similar (Table 1), which was expected as they had the same electrolyte conditions (indicating that all MFCs were strictly comparable in configuration). R_Ω depends on the ionic concentration, the type of ions and the electrode area. The differences in the R_Ω of different anodes (1.83–4.11 Ω) could be attributed to the differences in the active electrode area.

Compared to R_Ω, the R_{ct} changes with the frequency of the input signal. The different anode materials present different R_{ct}, which can be observed in their EIS response (Fig. 4). The R_{ct} is inversely proportional to the electron transfer rate. The CF1 presented a considerable R_{ct} (9.23 Ω), indicating that the system is kinetically sluggish compared to other anode materials employed in this study. EIS tests showed that the CF3 (2.60 Ω) had the lowest R_{ct}.

Low R_{ct} values indicated a higher activity on the electroactive sites because of a faster activation-controlled process at the anode–electrolyte interface, and hence a quicker electron transfer rate to the anode. Thus, CF3 could produce current up to higher power densities than the other anode configurations. CB exhibited the highest R_{ct} after CF1 (Table 1). This value of R_{ct} obtained for CB in our study is lower than R_{ct} (18 Ω) achieved by a previous study using CB as an anode and a wet-proofed carbon cloth as a cathode.[32] Another EIS study found that R_{ct} was the major internal resistance component in a brush anode MFC with a stainless-steel mesh Pt-catalysed cathode.[33] It must be considered that resistance values from other works cannot be directly compared because they depend on the type of cell used, the dimensions of the electrode and many other factors.

CG showed a small R_{ct} and displayed only a minimal frequency region where the mass transfer is a significant factor (linear response zone at impedance measurement). This mass transport limitation indicates that organic substrates could not reach the electrode surface for ARB feeding. The good compactness of the CG anode might have obstructed the anolyte circulation.

Adopting appropriate approaches to overcome internal resistance, R_Ω and R_{ct}, is essential to enhancing the performance of BES. Moreover, the biofilm formation on the anode surface should significantly modify cell performance by decreasing R_{ct}.

MFC performance during start-up

The start-up period of four selected carbon-based anodes (CF1, CF2, CF3 and CB) using two different inoculation strategies is shown in Fig. 5 as current output and in Supporting Information Fig. S2 as current density. The PA strategy resulted in a higher (except for CB) and earlier maximum current than the ER strategy. These results confirm that a positive anode potential promotes rapid microbial colonization due to increased energy yield per acetate oxidized. These results are consistent with Finkelstein *et al.*[34] in which the potential applied to the anode promoted the enrichment of specific consortia, and a more positive fixed potential resulted in a larger current output.

Table 2 summarizes the main results achieved for each anode in terms of maximum intensity, coulombic efficiency (CE) and days required to reach 0.5 mA of current generation. In the start-up phase using CB as the anode, the current was generated in 5 and 9 days for CB-PA and CB-ER, respectively. CB-ER showed better performance concerning the current generation, achieving a maximum of 6.6 mA (Table 2).

For MFCs using CF3 as the anode, a stepwise increase in current was also observed in these cycles, but PA configuration helped shorten the acclimation time. The maximum current generated by CF3-PA was 5 mA at day 37. In contrast, CF3-ER generated a similar current at day 44, indicating that the start-up of MFC with anodic positive fixed potential had effectively collected ARB with high electrochemical activity. These data implied that the PA-operated cells were able to have superior electrochemical activity during the start-up period compared to ER cells. This result is consistent with a study in which a higher maximum current was obtained using a PA of +200 mV than that of the control MFC operated under 1000 Ω.[26] However, the difference in the amount of current output obtained from different strategies in our study was not significant.

The start-up period was longer for MFCs employing CF1 as the anode, but also in this case PA was a faster strategy than ER. CF1-PA required 12 days to reach a current of 0.5 mA, while CF1-ER required 15 days. Lastly, the start-up time for CF2-PA was 2 days, and CF2-ER required 7 days to generate the current. No comparison was made for the inoculation phase of CG using both strategies due to the continuous disturbance in the current output obtained when the anode potential was fixed.

Regarding the CE performance (Table 2), the values obtained were high (81 ± 11%), indicating that only about 19% of the acetate consumed resulted in products other than ARB activity. These high CE values were also linked to a very high acetate removal efficiency of about 96%. Higher CE values were obtained for PA cells than for ER cells for all the anodes studied except for CF2. Then, the selection pressure due to the applied anode potential was useful to provide a better CE.

Overall, PA was demonstrated to be an efficient approach to reduce the start-up time of the MFCs, but its application requires special equipment, which affects the cost efficiency of the system. Working with ER can be more practical and economical than PA, since it does not require a potentiostat, facilitating field applications, while the results after the start-up period are of similar order.

Polarization curves

A polarization curve yields the overall fuel cell behaviour under specific operating conditions. To be precise, maximum power and resistance to current flow through the cell can be estimated by polarization tests. Figure 6(A) and Supporting Information Fig. S3(A) illustrate polarization curves obtained to compare MFC performance using different anode materials. The shape of the polarization curves obtained for each anode material displayed the three expected zones, starting from activation loss followed by ohmic loss and, finally, concentration or mass loss. The result indicated that mass transfer limited the performance of MFC with all electrodes employed in this study under high demand of current, because of the lower content of microorganisms available to produce electricity and the more difficult access of substrate to the points of the surface of the anode in which microorganisms had adhered.

The internal resistance was calculated by considering the linear relationship of the intensity–voltage curve. The internal resistance of each cell is summarized in Table 1. CB and CF3 presented the lowest internal resistance (111 and 122 Ω, respectively), while CF2 had approximately two times higher internal resistance than the previous materials. Since all the other parameters, including inoculum, medium and substrate, were kept the same, this higher internal resistance is assumed to be caused by the intrinsic

Journal of Chemical Technology and Biotechnology published by John Wiley & Sons Ltd on behalf of Society of Chemical Industry (SCI).

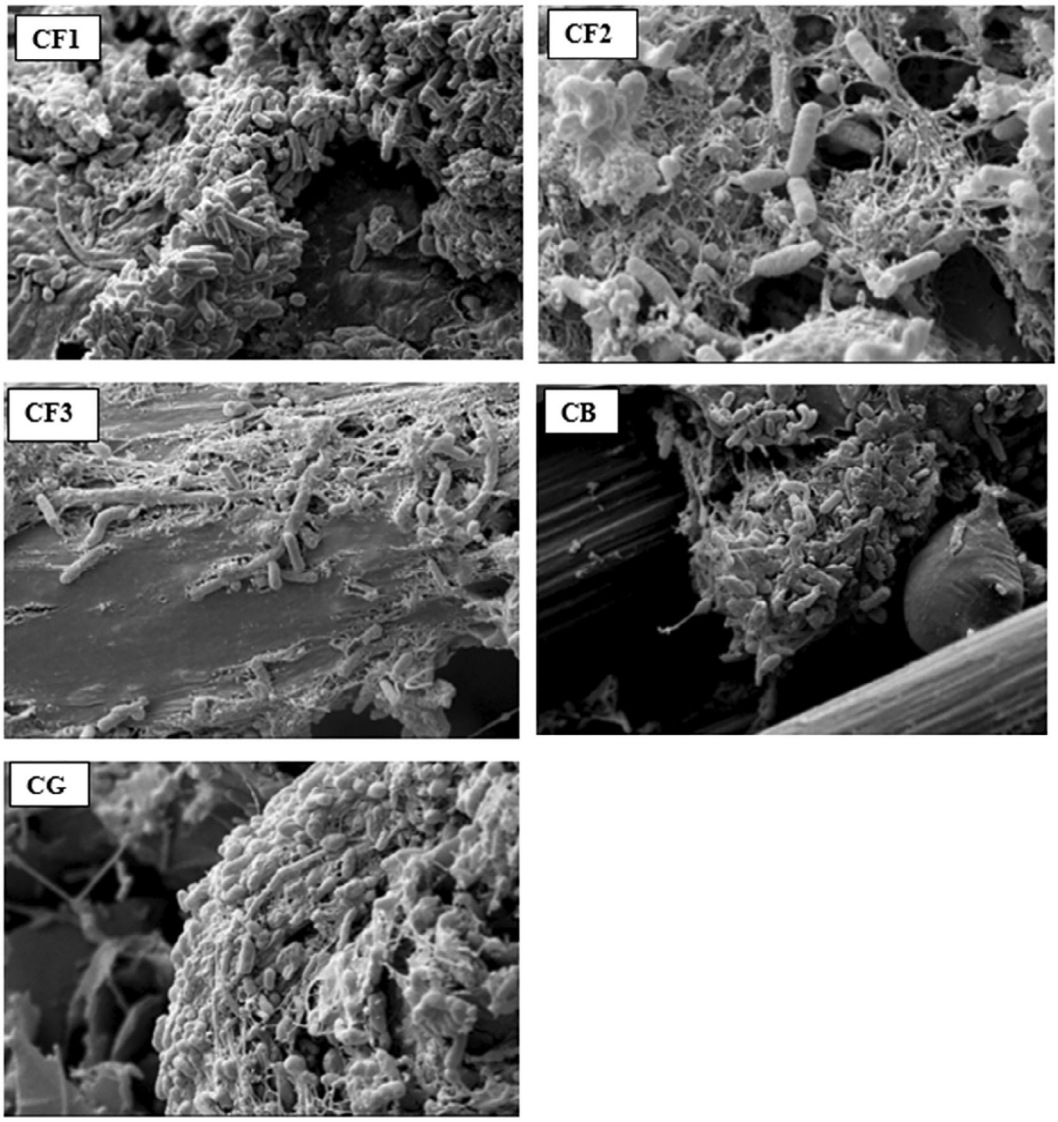

Figure 8. Scanning electron microscopy images on different carbon-based anode materials after biofilm formation. CF1, thicker carbon felt; CF2, high-conductivity carbon felt; CF3, high-active-area carbon felt; CB, carbon brush; CG, carbon granules.

properties of anode materials such as electrical conductivity, surface electroactive area, roughness and bacterial immobilization obtained.

Based on the power curves obtained (Fig. 6(B) and Supporting Information Fig. S3(B)), in agreement with polarization curves, a maximum power of 835 and 751 mW was achieved for CF3 and CB, respectively. The maximum power for other anode materials was almost half compared to the previous ones (Table 1). This result was expected because the CF3 and CB electrodes also presented higher maximum intensity than other carbonaceous anode materials, as observed with the CVs.

These significant differences in power may result from the amount of biomass adhering to each electrode and their different characteristics such as conductivity and roughness. The power curve obtained using the CF3 anode exhibited a steep drop in voltage at a higher current, resulting in power overshoot occurrence. There are few commonly accepted hypotheses regarding the power overshoot phenomenon in power curves. One theory on the cause of this power overshoot is that, as the current resistance decreases, the bacteria adhering to the anode cannot produce sufficient current at lower voltages.[27,35] Another reason might be the local acidification because diffusive proton transport from the biofilm has been reported to restrict the current density.[24] The acidification of the biofilm happens at higher current densities, which causes abrupt pH gradients inside the biofilm and limits the current production.[36] Given the nature of our experiments, the overshoot might have resulted from electron transfer limitations at the anode. This limitation is most likely related to the intrinsic property of the CF3 anode because other anodes used in this study did not exhibit power overshoot. Nevertheless, further experiments should be conducted to confirm the reason behind the power overshoot presented by the CF3 electrode.

Long-term evaluation of MFC performance for carbon-based anode materials

A set of six new MFCs with ER to close the circuit, each with a different anode electrode material, was evaluated for the long term (i.e., more than 2 months) under the same operating and feeding

Journal of Chemical Technology and Biotechnology published by John Wiley & Sons Ltd on behalf of Society of Chemical Industry (SCI).

conditions. Five of the MFCs used the same anodes as in the previous sections, and a different configuration named CF3 circularly stacked was tested in the sixth one and is discussed separately at the end of this section.

As can be observed in Supporting Information Fig. S4 as current and Fig. S5 as current density, there was an apparent influence of the anode material and its electroactive area (Table 1) on the production of current (Table 3). Using CB as the anode, the cell intensity was more than twice the intensity produced by CF1, CG and CF2. CF3 showed an intermediate behaviour – worse than CB but better than the other three electrodes. Compared with other carbonaceous anode materials employed, CB exhibited the best results (Table 3 and Supporting Information Figs S4 and S5), obtaining the highest current output of approximately 7 mA (480 mW) after several batches, with a maximum CE of 85%.

Unlike other studies, we will also discuss the results considering electroactive areas and not the geometric surface areas, to reflect that not all geometric area is electroactive. The geometric area gives an idea of the prospective space that microorganisms can interact with but, depending on the type of material, it will not be directly related to the electroactive area of the electrode. The percentage of the electroactive geometric area depends on the roughness of the material and its conductive properties.

The high electroactive area of CB (2.02 cm^2) plays an essential role in high CE and current generation because it enhances bacterial growth on the anode surface. Following CB, CF3 (with the highest electroactive area of 2.93 cm^2) achieved a maximum cell intensity of 5.7 mA (325 mW) (Table 3) and a maximum CE of 94%. The better performance of CF3 was reflected in the current output, as well as in the EIS analysis and polarization curves (Table 1). These results also agree with other reports in the literature showing that cylindrical brush anodes generally produced higher current densities than flat carbon felt, carbon cloth and carbon paper anodes when coupled to a cathode with a platinum catalyst.[37]

It can also be observed (Supporting Information Fig. S4) that the intensity of CF2 incremented to a certain extent and evidenced a decrement after 40 operation days. This might occur due to the declination of electrochemical activity by degrading the anodic biofilm or possible biofouling, and therefore it is shown as the least appropriate anode material for long-term operation.

Even though the CF1 anode had the lowest maximum intensity compared to other anode materials, it presented higher current density when normalized to the electroactive area (Table 3). After CF1, CB and CF3 obtained higher maximum current densities of 35.7 and 18.4 A m^{-2}, respectively. Despite the better current output, the maximum current density of CB and CF3 normalized to the electroactive area is much lower than the CF1 electrode due to its very low electroactive area. The current density for CF2 is not reported since its electroactive area could not be determined.

However, when the current densities are calculated normalized with the projected surface area (Table 3 and Supporting Information Fig. S5), CB and CF3 present the highest values, consistent with results obtained from the electrochemical techniques previously reported. In other works, the current density has been reported to exceed 20 A m^{-2} with graphite thin felt anode (projected surface area of 150 cm^2 and 0.4 cm thickness) and 0.5 mg Pt cm^{-2} carbon felt air-breathing cathode.[38]

Overall, these results confirm that CBs are more suitable for bacterial adhesion and electron transfer due to their configuration and electroactive area. Therefore, they have qualities that make them a very good option for scaling up MFC systems. Moreover, considering the long-term operation of MFCs, CB has an advantage over other carbonaceous anodes, such as carbon felt, which can become problematic because clogging the pores with biofilm can reduce its efficiency. On the other hand, because the brush contains very fine fibres with plenty of circulation room around them, dead bacteria do not clog the brush.[39] However, another frame of reference is that larger-scale BES require compact architectures to treat wastewater efficiently. In this scenario, CF3 carbon felt could be a good alternative, with nearly similar performance.

Besides the nature of the material, CB and carbon felt have different shapes that can also affect the performance of the cells working with these anodes. This fact makes the comparison between these anodes a bit unfair. A similar geometry to CB of carbon felt anode was studied to create a more reasonable and fair comparison. Since among the three carbon felt anodes employed in this study CF3 presented better results, another configuration for CF3 was investigated. The CF3 material was cut into small circles and then stacked vertically, simulating the geometric shape of the CB. The circularly stacked CF3 design had a maximum current output of 7.2 mA (Table 3 and Supporting Information Fig. S4), similar to the CB and higher than the rectangular CF3 design, due to their larger surface area and closer electrode spacing. Comparing the current density normalized to the anode surface area against rectangular CF3, the circularly stacked CF3 had the maximum current density of 16.4 A m^{-2} – better than CF3 (14.3 A m^{-2}) and slightly higher than CB (15.9 A m^{-2}). In summary, these results show that CF3 material can provide CB-like performance when using CB-like geometry.

MEC performance of carbon-based anode materials

After obtaining the results reported above, the anodes were transferred to MEC operation for 40 days. For each anode material, the performance obtained in terms of current intensity is presented in Supporting Information Fig. S6 as current and Fig. S7 as current density. Hydrogen production rate, CE, r_{cat} and maximum intensity are reported in Table 4. The current intensity in MEC decreased regarding MFC operation for CF1, CF2 and CF3 (Supporting Information Fig. S6), indicating lower exoelectrogenic activity, which is common when switching from MFC to MEC. During MFC operation, the cathode is aerobic and therefore there is a chance of oxygen intrusion to the anode, which can affect the microbial community present on the anode.[40] On the other hand, in MEC, the cathode was kept under anaerobic conditions, leading to the presence of strict anaerobic bacteria in the system. Apart from that, the pH of the solution in MEC could change due to hydrogen production affecting its microbial community as well. Other factors can also influence the current density in MEC (cathodic catalysts, applied voltage, ohmic resistance and so on).[41,42] For example, the limitations in current density due to cathodic reaction and ohmic resistance could be attenuated by using better materials and improving reactor design. Nevertheless, more studies should be performed to identify the main limiting factor for current densities in MEC.

The highest current intensity in MEC was observed for CB, reaching about 7.5 mA. A similar current intensity of 7.3 mA was measured on average for MEC with CF3 circularly stacked. The current CB and CF3 stacked intensity trend circularly correlated well with the better performance observed in MFC operation.

As expected, the maximum hydrogen gas production rates (Table 4) varied for the different anode materials and remained the highest at 1.04 m^3 H_2 m^{-3} d^{-1} for CB and 0.92 m^3

Journal of Chemical Technology and Biotechnology published by John Wiley & Sons Ltd on behalf of Society of Chemical Industry (SCI).

H_2 m^{-3} d^{-1} for CF3 stacked. The rates produced here are comparable to those in previous studies using similar carbon-based anodes.[27,35] To improve hydrogen production rate, previous works suggested the use of a buffer in the catholyte solution because it helps to maintain pH and reduces the cell internal resistance.[43]

Among the different types of anode materials, CB, CG and CF3 circularly stacked had the highest CE, as expected, based on the highest peak currents. The higher the current intensity, the less likely it is that the acetate will be consumed by other routes. These values indicate the high efficiency of capturing electrons from the acetate in the form of current.

The cathodic hydrogen recoveries (r_{cat}) were the largest for CB, CF3 and CF3 circularly stacked, with 90%, followed by 98% and 99%, respectively. A lower r_{cat} means that the generated electrons were lost to methane generation or other alternative reactions rather than recovery as hydrogen gas.[44] It is also worth mentioning that there was a decrease in r_{cat} at increased reaction times, which coincided with the loss of biogas purity, starting from high relative composition of hydrogen, and ending up enriched in methane. As a matter of fact, for each MEC, the composition of the gas collected for the last batch cycles entirely contained methane. Hydrogenotrophic methanogens were most likely responsible for low hydrogen gas recovery due to the high formation of methane. In any case, this is a typical problem observed when operating single-chamber MECs.[45]

Overall, considering the results obtained under MEC operation, it was concluded that CB and CF3 circularly stacked demonstrated better overall performance amongst the carbonaceous anodes.

Microbiological analysis

The microbial community analysis showed that the anode electrode material affected the enriched microbiome (Fig. 7). At the class level, the microbiomes on the electrodes producing the highest current, namely CB and CF3, were dominated by Desulfuromonadia, the relative abundances being 55.4–60.9% and 38.4–48.9%, respectively. The dominant family was Geoalkalibacteraceae, with relative abundances increasing to 60.9% in CB and 42.6% in CF3. *Geoalkalibacter* species have been reported to support efficient electricity generation in BES, especially under saline conditions.[46-48] The current densities have been reported to increase up to 8.5 A m^{-2}.[47]

On CF2 and CG, Gammaproteobacteria were detected at the highest abundance (45.4–52.4% and 31.8–32.4%). Over 16% of the microorganisms were closely related to *Nitrincola lacisaponensis*, while CF2 and CG samples also contained a significant abundance of *Azoarcus* sp. (around 9.4%) or *Halomonas* sp. (around 8.9%), respectively. Other studies also detected bacteria in *Nitrincola* genus from enriched electroactive biofilms.[49-51] Both samples also contained a significant abundance of Bacteroidia (17.3–23.2% and 15.5–18.3%, respectively). Over 24% of the bacteria on CG biofilm belonged to Alphaproteobacteria.

The community on CF1 was dominated by Chrysiogenetes (43.6–45.9%) and, while Desulfuromonadia (11.5–15.1%) were also detected, the samples also contained a significant abundance of Methanobacteria (16.8–21.6%), indicating that in this cell a significant amount of acetate was consumed for methanogenesis. The dominant family was Chrysiogenaceae (43.6–45.9%), and the dominant genus was detected to be sulfur- and nitrate-reducing *Desulfurispirillum*,[52] while *Geoalkalibacter* (11.5–15.0%) were also detected. Clostridia were seen to be present in all the samples, the abundances ranging from 2.4–2.6% in CF2 to 7.3–10.8% in CF3.

As a conclusion of the microbiological characterization of the different anodes, it was observed that the exoelectrogenic activity offered by the different anodes was highly correlated with the presence of ARB, specifically *Geoalkalibacter*.

Scanning electron microscopy

SEM was used for physical characterization of the biofilms on the carbon-based anode surface. Figure 8 displays the SEM images of the surface of the different anodes employed. The different biofilm structure on CB can be observed, where the biofilm colonized the carbon fibre brush with considerable thickness. More space exists between intersectional carbon fibre biofilm than a smooth and uniform biofilm structure on carbon felts. The fact that CB presents a porous structure may lead to better substrate access, resulting in high current density and explaining why the CB performs better in terms of current output. It is also noteworthy that, although the biofilm formed at the surface of CF3 contained less biomass than CF1 and CG, it showed a higher current density. Moreover, the developed biofilm on the CG showed different morphological characteristics from the biofilm on the carbon felt and CB electrodes. This result can be mainly attributed to different CG structures than other electrodes with different fibre arrangements. Also, the heterogeneous nature of the microbial population in the inoculum can be observed.

It can also be noted that the biofilm did not cover the electrode surface in all cases and showed extensive voids, especially for CF2. The biofilm presented by CB was relatively compact and showed fewer voids. Therefore, it is the most appropriate since it has been reported that gaps in the biofilm structure may result in reduced contact for the transfer of electrons and consequently decrease MFC performance.[43] However, it should also be mentioned that void spaces are beneficial for mass transport within the biofilm structure by making water channels that aid the substrate supply.[53] Based on these results from the surface SEM images, it is evident that the CB and CF1 presented visually compact and dense structures in which microorganisms are embedded in extracellular polymeric substances. It can also be observed that, although CF3 showed better overall performance than some other anode materials, it had visually less amount of biomass on the surface. This thin and open biofilm structure of CF3 may allow for a sufficient substrate migration without hampering electron transfer to the anode. This might explain the high activity but low biomass on the surface.

Indeed, using carbon materials as anodes with a high microbially accessible surface area is beneficial for MFCs. However, other factors like the electrode material cost, required space and liability to clogging must be considered.

CONCLUSIONS

Different carbon-based materials as bioanodes and two different start-up strategies were studied in this work. During the start-up phase, the current output of PA was better than ER due to the increase of substrate oxidation driving force. PA demonstrated a slightly more efficient approach for the faster start-up than ER, suggesting that a poised applied potential of 200 mV during biofilm enrichment affects the electron transfer mechanism. However, operating various MFCs continuously at a fixed potential during real-world conditions will have some practical implications as it would require an expensive multichannel potentiostat, while

Journal of Chemical Technology and Biotechnology published by John Wiley & Sons Ltd on behalf of Society of Chemical Industry (SCI).

the results obtained during stable operation are very similar to those with ER.

Based on the results obtained for carbonaceous anodes, CB and CF3, both rectangular and circularly stacked cylindrically, were the optimum anode as they were effective in terms of maximum current intensity, CE, hydrogen production rate and cathodic recovery efficiency. The better performance of these anodes was consistent with CV, EIS and polarization tests, which showed the maximum intensity and lower internal resistance of CB and CF3 than the other carbon-based anode materials tested.

The microbial community analysis results and SEM indicated that the materials demonstrating the highest electricity production efficiencies in the performance analysis (CB and CF3) supported the development of efficient electroactive biofilms with a high fraction of *Geoalkalibacter*, which enhanced the CE and hydrogen production rate.

ACKNOWLEDGEMENTS

This work was supported by Grant CTQ2017-82404-R funded by MCIN/AEI/10.13039/501100011033 and by ERDF A way of making Europe. The authors are members of the GENOCOV research group (Grup de Recerca Consolidat de la Generalitat de Catalunya, 2021 SGR 515, www.genocov.com). The authors wish to thank Alfons Miàs and Anna Alcon (Open Labs UAB) for their great assistance with 3D printers and Leitat technological centre, and National Hydrogen and Fuel cell technology testing centre for providing the carbon felt samples.

CONFLICT OF INTEREST

The authors declare that they have no conflict of interest.

SUPPORTING INFORMATION

Supporting information may be found in the online version of this article.

REFERENCES

1 Sánchez-Peña P, Rodriguez J, Montes R, Baeza JA, Gabriel D, Baeza M *et al.*, Less is more: a comprehensive study on the effects of the number of gas diffusion layers on air–cathode microbial fuel cells. *ChemElectroChem* **8**:3416–3426 (2021).
2 Flimban SGA, Ismail IMI, Kim T and Oh S-E, Overview of recent advancements in the microbial fuel cell from fundamentals to applications: design, major elements, and scalability. *Energies* **12**:3390 (2019).
3 Bhargavi G, Venu V and Renganathan S, Microbial fuel cells: recent developments in design and materials. *IOP Conf Ser: Mater Sci Eng* **330**:012034 (2018).
4 Kalathil S, Patil SA and Pant D, Microbial Fuel Cells: Electrode Materials, in *Encyclopedia of Interfacial Chemistry*, Vol. **309–318**. Elsevier, Amsterdam, Netherlands (2018). https://doi.org/10.1016/B978-0-12-409547-2.13459-6.
5 Zhou M, Chi M, Luo J, He H and Jin T, An overview of electrode materials in microbial fuel cells. *J Power Sources* **196**:4427–4435 (2011).
6 Wei J, Liang P and Huang X, Recent progress in electrodes for microbial fuel cells. *Bioresour Technol* **102**:9335–9344 (2011).
7 Miceli JF, Parameswaran P, Kang D-W, Krajmalnik-Brown R and Torres CI, Enrichment and analysis of anode-respiring bacteria from diverse anaerobic Inocula. *Environ Sci Technol* **46**:10349–10355 (2012).
8 Do MH *et al.*, Challenges in the application of microbial fuel cells to wastewater treatment and energy production: a mini review. *Sci Total Environ* **639**:910–920 (2018).
9 Torres CI, Krajmalnik-Brown R, Parameswaran P, Marcus AK, Wanger G, Gorby YA *et al.*, Selecting anode-respiring bacteria based on anode potential: phylogenetic, electrochemical, and microscopic characterization. *Environ Sci Technol* **43**:9519–9524 (2009).
10 Zhu X, Yates MD, Hatzell MC, Ananda Rao H, Saikaly PE and Logan BE, Microbial community composition is unaffected by anode potential. *Environ Sci Technol* **48**:1352–1358 (2014).
11 Rabaey K, Boon N, Siciliano SD, Verhaege M and Verstraete W, Biofuel cells select for microbial consortia that self-mediate electron transfer. *Appl Environ Microbiol* **70**:5373–5382 (2004).
12 Vishwanathan AS *et al.*, Carbon quantum dots shuttle electrons to the anode of a microbial fuel cell. *3 Biotech* **6**:228 (2016).
13 Liu X-W, Sun XF, Chen JJ, Huang YX, Xie JF, Li WW *et al.*, Phenothiazine derivative-accelerated microbial extracellular electron transfer in bioelectrochemical system. *Sci Rep* **3**:1616 (2013).
14 Dennis PG, Virdis B, Vanwonterghem I, Hassan A, Hugenholtz P, Tyson GW *et al.*, Anode potential influences the structure and function of anodic electrode and electrolyte-associated microbiomes. *Sci Rep* **6**:39114 (2016).
15 Schröder U, Anodic electron transfer mechanisms in microbial fuel cells and their energy efficiency. *Phys Chem Chem Phys* **9**:2619–2629 (2007).
16 Yaqoob AA, Ibrahim MNM and Rodríguez-Couto S, Development and modification of materials to build cost-effective anodes for microbial fuel cells (MFCs): an overview. *Biochem Eng J* **164**:107779 (2020).
17 Dumitru A and Scott K, Anode materials for microbial fuel cells, in *Microbial Electrochemical and Fuel Cells*, Vol. **117–152**. Elsevier, Amsterdam, Netherlands (2016). https://doi.org/10.1016/B978-1-78242-375-1.00004-6.
18 Yaqoob AA, Mohamad Ibrahim MN, Rafatullah M, Chua YS, Ahmad A and Umar K, Recent advances in anodes for microbial fuel cells: an overview. *Materials* **13**:2078 (2020).
19 Ketep SF, Bergel A, Calmet A and Erable B, Stainless steel foam increases the current produced by microbial bioanodes in bioelectrochemical systems. *Energy Environ Sci* **7**:1633–1637 (2014).
20 Aelterman P, Freguia S, Keller J, Verstraete W and Rabaey K, The anode potential regulates bacterial activity in microbial fuel cells. *Appl Microbiol Biotechnol* **78**:409–418 (2008).
21 Wei J, Liang P, Cao X and Huang X, A new insight into potential regulation on growth and power generation of *Geobacter sulfurreducens* in microbial fuel cells based on energy viewpoint. *Environ Sci Technol* **44**:3187–3191 (2010).
22 Kracke F, Vassilev I, Krömer JO and Microbial electron transport and energy conservation, The foundation for optimizing bioelectrochemical systems. *Front Microbiol* **6**:575 (2015).
23 Lee H-S, Torres CI and Rittmann BE, Effects of substrate diffusion and anode potential on kinetic parameters for anode-respiring bacteria. *Environ Sci Technol* **43**:7571–7577 (2009).
24 Torres CI, Kato Marcus A and Rittmann BE, Proton transport inside the biofilm limits electrical current generation by anode-respiring bacteria. *Biotechnol Bioeng* **100**:872–881 (2008).
25 Wagner RC, Call DF and Logan BE, Optimal set anode potentials vary in bioelectrochemical systems. *Environ Sci Technol* **44**:6036–6041 (2010).
26 Wang X, Feng Y, Ren N, Wang H, Lee H, Li N *et al.*, Accelerated start-up of two-chambered microbial fuel cells: effect of anodic positive poised potential. *Electrochim Acta* **54**:1109–1114 (2009).
27 Zhu X, Tokash JC, Hong Y and Logan BE, Controlling the occurrence of power overshoot by adapting microbial fuel cells to high anode potentials. *Bioelectrochemistry* **90**:30–35 (2013).
28 Call D and Logan BE, Hydrogen production in a single chamber microbial electrolysis cell lacking a membrane. *Environ Sci Technol* **42**:3401–3406 (2008).
29 Middaugh, J., Cheng, U. S. & Liu, W. How to make cathodes with a diffusion layer for single-chamber microbial fuel cells.
30 Cheng S, Liu H and Logan BE, Power densities using different cathode catalysts (Pt and CoTMPP) and polymer binders (Nafion and PTFE) in single chamber microbial fuel cells. *Environ Sci Technol* **40**:364–369 (2006).
31 Baeza JA, Advanced direct digital control (AddControl): lessons learned from 20 years of adding control to lab and pilot scale treatment systems, in *13th IWA Conference on Instrumentation, Control and Automation*. ICA 2022 13–15. Tsinghua University, Beijing (China) (2022).

Journal of Chemical Technology and Biotechnology published by John Wiley & Sons Ltd on behalf of Society of Chemical Industry (SCI).

32 Hutchinson AJ, Tokash JC and Logan BE, Analysis of carbon fiber brush loading in anodes on startup and performance of microbial fuel cells. *J Power Sources* **196**:9213–9219 (2011).
33 Zhang F, Merrill MD, Tokash JC, Saito T, Cheng S, Hickner MA *et al.*, Mesh optimization for microbial fuel cell cathodes constructed around stainless steel mesh current collectors. *J Power Sources* **196**:1097–1102 (2011).
34 Finkelstein DA, Tender LM and Zeikus JG, Effect of electrode potential on electrode-reducing microbiota. *Environ Sci Technol* **40**:6990–6995 (2006).
35 Watson VJ and Logan BE, Analysis of polarization methods for elimination of power overshoot in microbial fuel cells. *Electrochem Commun* **13**:54–56 (2011).
36 Erben J, Pinder ZA, Lüdtke MS and Kerzenmacher S, Local acidification limits the current production and biofilm formation of Shewanella oneidensis MR-1 with electrospun anodes. *Front Microbiol* **12**: 660474 (2021).
37 Zhao Y, Ma Y, Li T, Dong Z and Wang Y, Modification of carbon felt anodes using double-oxidant HNO_3/H_2O_2 for application in microbial fuel cells. *RSC Adv* **8**:2059–2064 (2018).
38 Erable B, Etcheverry L and Bergel A, Increased power from a two-chamber microbial fuel cell with a low-pH air-cathode compartment. *Electrochem Commun* **11**:619–622 (2009).
39 Zhang L, Zhu X, Li J, Liao Q and Ye D, Biofilm formation and electricity generation of a microbial fuel cell started up under different external resistances. *J Power Sources* **196**:6029–6035 (2011).
40 Montpart N, Rago L, Baeza JA and Guisasola A, Oxygen barrier and catalytic effect of the cathodic biofilm in single chamber microbial fuel cells. *J Chem Technol Biotechnol* **93**:2199–2207 (2017).
41 Dhar BR and Lee H-S, Evaluation of limiting factors for current density in microbial electrochemical cells (MXCs) treating domestic wastewater. *Biotechnol Rep* **4**:80–85 (2014).
42 Ruiz Y, Baeza JA and Guisasola A, Microbial electrolysis cell performance using non-buffered and low conductivity wastewaters. *Chem Eng J* **289**:341–348 (2016).
43 Ribot-Llobet E, Nam J-Y, Tokash JC, Guisasola A and Logan BE, Assessment of four different cathode materials at different initial pHs using unbuffered catholytes in microbial electrolysis cells. *Int J Hydrogen Energy* **38**:2951–2956 (2013).
44 Ruiz Y, Baeza JA and Guisasola A, Revealing the proliferation of hydrogen scavengers in a single-chamber microbial electrolysis cell using electron balances. *Int J Hydrogen Energy* **38**:15917–15927 (2013).
45 Rago L, Ruiz Y, Baeza JA, Guisasola A and Cortés P, Microbial community analysis in a long-term membrane-less microbial electrolysis cell with hydrogen and methane production. *Bioelectrochemistry* **106**: 359–368 (2015).
46 Yadav S and Patil SA, Microbial electroactive biofilms dominated by Geoalkalibacter spp. from a highly saline–alkaline environment. *npj Biofilms Microbiomes* **6**:38 (2020).
47 Pierra M, Carmona-Martínez AA, Trably E, Godon J-J and Bernet N, Specific and efficient electrochemical selection of Geoalkalibacter subterraneus and Desulfuromonas acetoxidans in high current-producing biofilms. *Bioelectrochemistry* **106**:221–225 (2015).
48 Badia-Fabregat M, Rago L, Baeza JA and Guisasola A, Hydrogen production from crude glycerol in an alkaline microbial electrolysis cell. *Int J Hydrogen Energy* **44**:17204–17213 (2019).
49 Daghio M, Gandolfi I, Bestetti G, Franzetti A, Guerrini E and Cristiani P, Anodic and cathodic microbial communities in single chamber microbial fuel cells. *N Biotechnol* **32**:79–84 (2015).
50 Rago L, Baeza JA and Guisasola A, Increased performance of hydrogen production in microbial electrolysis cells under alkaline conditions. *Bioelectrochemistry* **109**:57–62 (2016).
51 Mao Z, Cheng S, Sun Y, Lin Z, Li L and Yu Z, Enhancing stability and resilience of electromethanogenesis system by acclimating biocathode with intermittent step-up voltage. *Bioresour Technol* **337**: 125376 (2021).
52 Sorokin DY, Foti M, Tindall BJ, Muyzer G and Desulfurispirillum alkaliphilum gen. nov. sp. nov, A novel obligately anaerobic sulfur- and dissimilatory nitrate-reducing bacterium from a full-scale sulfide-removing bioreactor. *Extremophiles* **11**:363–370 (2007).
53 Cheng S, Liu H and Logan BE, Increased performance of single-chamber microbial fuel cells using an improved cathode structure. *Electrochem Commun* **8**:489–494 (2006).

Journal of Chemical Technology and Biotechnology published by John Wiley & Sons Ltd on behalf of Society of Chemical Industry (SCI).